Combined EEffects of Nanoparticles andon Surfactants uponin Controlling Foam StabilitySynergy Between Nanoparticles and Surfactants in Controlling Foam Stability

Mohammad Javad Shojaei[1], Yves Méheust[2], Abdulkadir Osman[3], Paul Grassia[4], and Nima Shokri*[5]

[1]Department of Earth Science and Engineering, Imperial College London, London, United Kingdom

[2]Université de Rennes, CNRS, Géosciences Rennes, UMR 6118, 35000 Rennes, France

[3]Department of Chemical Engineering and Analytical Science, The University of Manchester, Manchester, UK

[4]Department of Chemical and Process Engineering, University of Strathclyde, Glasgow G1 1XJ, United Kingdom

[5]Hamburg University of Technology, Institute of Geo-Hydroinformatics, Am Schwarzenberg-Campus 3 (E), 21073 Hamburg, Germany

*Corresponding Author

Prof. Nima Shokri

Email: nima.shokri@tuhh.de

Website: www.tuhh.de/ghi

Abstract

We investigate the effect of surfactants with different charges (anionic, cationic, and non-ionic) on foam stability in the presence of charge-stabilized silica (SiO_2) nanoparticles. Toward this aim, a comprehensive series of experiments on a Hele-Shaw cell and a foam column is conducted at bubble and bulk-scale respectively, that is, investigating phenomenologies of foam coarsening separately by gas diffusion and bubble coalescence, and by gravitational drainage. Our results show nanoparticles, despite their ability to position themselves at liquid-gas interfaces and thus limit the resulting surface tension coefficient, do not necessarily have a positive effect on foam stability; the nature and magnitude of this effect depends strongly on the nature of the surfactant, its concentration and the concentration of nanoparticles. In less stable systems, significant coarsening ~~by bubble coalescence~~ occurs. Both results from bubble-scale and the bulk-scale experiments suggest that compatibility experiments are pre-requisite to foam stability analysis to test the compatibility between surfactants and nanoparticles.

Keywords: Foam stability, Diffusional coarsening, Bubble coalescence, Gravitational drainage, Nanoparticle, Surfactant~~, Bubble and Bulk scale~~.

Introduction

Gas injection into subsurface reservoirs is a common practice in many industrial and engineering processes such as enhanced oil recovery (EOR), CO_2 sequestration and soil remediation (Benson and Cole, 2008; Blunt et al., 1993; Feng et al., 2012; Kantzas et al., 1988). In most cases, viscous fingering and gravity override due to unfavourable viscosity and density ratios between the gas and the resident liquid(s), and preferential flow of gas due to reservoirs heterogeneity, are responsible for low sweep efficiency (Chang et al., 1994; Garcia and Pruess, 2003). Foams, which are dispersions of a large volume of gas in a liquid such that the gas phase is made discontinuous by films of the liquid phase denoted lamellae (Hirasaki et al., 1997a; Kam and Rossen, 2003; Shojaei et al., 2018a), are a promising potential remedy to these complications (Hirasaki and Lawson, 1985; Shojaei et al., 2019). The apparent viscosity of foam can be up to 1000 times higher than that of its constituents, which makes foams ideal for fluid displacement (Hirasaki et al., 1997b; Shojaei et al., 2018b).

In general, foams are classified into two categories, which are typically known as *bulk foam* and *confined foam* (Rossen, 1996), based on the size of bubbles relative to the typical length scale of the confined media (e. g., the average pore size or channel width). foam can be considered a *bulk foam* when the dimension of the confining space is significantly larger than the typical bubble size. On the other hand, the foam is *confined foam* when the bubbles have the same size or are larger than the characteristic length scale of the confining space. Foams exhibit two different geometries depending on their quality, i. e., their gas content (Ma et al., 2012). In wet systems (i.e., at low foam qualities), the lamellae are thick, the foam bubbles have a quasi-spherical shape, and the foams are fine-textured, whereas, at higher foam quality, the lamellae are thinner and foam bubbles tend to have a more polyhedral shape.

The stability of a foam refers to its capacity to retain its geometry/topology over a significant amount of time despite not being stable thermodynamically. In porous media applications involving non-aqueous phase liquids (NAPLs), such as foam EOR or foam-based remediation of NAPL-contaminated aquifers and soils, the foam's texture evolves irreversibly in time as a consequence of four different processes: (1) gas diffusion (2), liquid drainage (3), interaction with oil/NAPL and (4) capillary suction (Ma et al., 2012; Osei-Bonsu et al., 2015; Rossen, 1996){Rossen, 1996 #2512}. In the capillary suction mechanism, when the capillary pressure (the pressure across the interface between the gas and the surfactant solution) increases, the lamellae thickness decreases, eventually causing it to break if a threshold in capillary pressure is exceeded. That threshold is called the maximum capillary pressure beyond which coalescence (i.e., appearance of a larger bubble as a result of the breakage of film between two smaller bubbles) occurs.

Adjacent foam bubbles do not have the same size, and hence the gas is at different pressures inside the bubbles. The gas in smaller foam bubbles is at a higher pressure than the gas in larger ones. Indeed, the bubble radius controls the pressure inside the bubbles as a consequence of the Young–Laplace equation, which relates the pressure difference ΔP across a fluid interface to the surface tension coefficient σ and the principal radii of curvature r_1 and r_2 according to $\Delta P = \sigma\left(\frac{1}{r_1}+\frac{1}{r_2}\right)$ (Lemlich, 1978). Gas thus diffuses from the small bubbles with higher pressure to larger bubbles with lower pressure, which eventually causes the disappearance of neighbouring small bubbles (Blijdenstein et al., 2010; Maestro et al., 2014; Saint-Jalmes, 2006). This phenomenon is called gas diffusion ~~on~~ coarsening.

Liquid drainage is a multistage process consisting of (a) liquid flow from the lamellae to the Plateau border (which are the lamellae's intersections) due to capillary suction, (b) liquid

release from the coalescence of foam bubbles, and (c) downward liquid drainage along Plateau borders under the effect of gravity, resulting in accumulation of liquid in the lower layer of the foam (Exerowa and Kruglyakov, 1997). The entire process is mainly controlled by gravity and capillary suction and eventually leads to film breakage~~rupture~~s (and, hence, ~~/~~bubble coalescence) as the thickness of lamellae falls below a certain value (Bhakta and Ruckenstein, 1997). Drainage, therefore, presents a challenge for foam-based displacement processes.

Another major challenge to the effective utilization of foam application in oil displacement is the adverse effect of oil on foam stability as a result of direct surface interactions between oil and foam, which leads to aqueous film thinning and breakage~~rupture~~ (Koczo et al., 1992; Nikolov et al., 1986; Osei-Bonsu et al., 2018). The negative effect of oil on foam stability depends on the properties of the surfactant and oil. Light oil (small hydrocarbon chains) has been found to be more detrimental to foam stability than heavier oil (long hydrocarbon chains) (Lobo et al., 1989; Talebian et al., 2013).

In view of the above-mentioned challenges to foam stability, in recent years, there has been a growing interest in the joint utilization of nanoparticles and surfactant to stabilize foams (Karakashev et al., 2011; Kumar and Mandal, 2017; Maestro et al., 2014; Yekeen et al., 2018; Yu et al., 2012b). The effective contribution of nanoparticles to foam stability is attributed to the adsorption and accumulation of nanoparticles at the gas-liquid interfaces of foam bubbles and Plateau borders (Yekeen et al., 2018). Nanoparticles reduce the direct contact between the fluids, which decelerates the gas diffusion rate and bubble bursting (Karakashev et al., 2011; Maestro et al., 2014; Yu et al., 2012b), and film drainage is slowed as well due to the presence of the nanoparticles. The lower tendency of nanoparticles (compared to the surfactant) to adsorb on reservoir rocks is another reason that makes them a desirable foam stabilizer (Yekeen et al., 2018). Nanoparticles are well suited to subsurface applications.

Their small size limits the possibility of pore plugging as they pass through the pore throats in porous media (Yu et al., 2012b). Their solid nature also makes them highly resistant to the harsh condition of reservoirs such as high pressure and temperature, high salinity and the presence of oil (Yusuf et al., 2013; Zhang et al., 2009). Also, nanoparticles can be functionalized with different chemical groups to improve their aqueous stability and tune the wettability of the solutions, or coated for different purposes such as increasing their CO_2 solvation capability and capability to adhere to the fluid-gas interface, which contributes to improving the foam's stability (Panthi et al., 2017; Singh and Mohanty, 2017).

In addition to the decrease in gas diffusion and liquid drainage, the main proposed causes for the increase in foam stability when using nanoparticles are an increase in particle detachment energy and in the maximum capillary pressure for bubble~~foam~~ coalescence (Yekeen et al., 2018). The particle detachment energy is the energy required for the removal of individual nanoparticles from lamellae (Singh and Mohanty, 2015). The adsorption of nanoparticles at the interface is thus considered irreversible due to their large detachment energy, while other conventional foaming agents can easily adsorb and desorb from the gas-liquid interface of foam bubbles. Therefore, the presence of the adsorbed SiO_2 nanoparticles, by increasing the lamellar stability, ~~–~~increases the maximum capillary pressure beyond which coalescence occurs (Yekeen et al., 2018). This increase in maximum capillary pressure depends on nanoparticle concentration and on how they agglomerate at the gas-liquid interface.

The presence of nanoparticles at the gas-liquid interface decreases the surface tension~~interfacial tension~~ of foam bubbles with respect to conventional foams (Kantzas et al., 1988), and hence decreases the capillary pressure. Consequently, the pressure differences between adjacent bubbles decrease in the presence of nanoparticle and gas diffusion decreases accordingly, while the permeability of the film to gas decreases also. Also, the fact that the surface tension of the surfactant solution decreases~~Also, the surface tension of the~~

~~surfactant solution decreases~~ in the presence of silica nanoparticle (Jia et al., 2020; Vatanparast et al., 2018) that could potentially improve foam stability and foam generation.

Nanoparticles can be arranged at the gas-liquid interface as a monolayer, bilayer, or a network of particles based on their surface wettability (Bi et al., 2004; Horozov, 2008). The resistance of nanoparticles to exit the interface controls the stability of a monolayer nanoparticle arrangement (Kantzas et al., 1988), while the stability of a bilayer and network of nanoparticles arrangement is influenced by interfacial rheological properties and by the capillary pressure (Kantzas et al., 1988). Generally, a network of nanoparticles provides higher stability by forming thick solid lamellae that prevent film thinning and gas diffusion more effectively by increasing the surfactant solution's viscosity and decreasing gas diffusivity. In addition, liquid drainage and gravitational drainage could be decelerated in the presence of nanoparticles. Hence the arrangement of nanoparticles at the interface during liquid drainage is a key control parameter in foam stability enhancement by nanoparticles.

It has been claimed based on experimental data that in any given system, there is an optimal concentration of nanoparticles that improves foam stability to the largest extent (Espinoza et al., 2010). At low concentration, the presence of nanoparticles at the gas-liquid interface is not sufficient to achieve high stability. As the nanoparticle concentration is increased, more nanoparticles find themselves at the gas-liquid interfaces, which enhances foam stability by reducing foam drainage and liquid film thinning. However, foam stability either remains constant or decreases when the concentration passes a critical value (AttarHamed et al., 2014; Chen et al., 2014). It has been established that nanoparticles, irrespective of the type, have a significant influence on static and dynamic stability of foam (Yekeen et al., 2018). What is not yet clearly understood is how the nature of the surfactant affects foam stability in the presence of nanoparticles. To improve our physical understanding of the interaction between nanoparticles and surfactants in determining foam stability,~~To improve our physical~~

~~understanding of the synergy between nanoparticles and surfactants on foam stability,~~ in this study we investigate the impact of nanoparticles in the presence of surfactants with varying charges (anionic, cationic, and non-ionic) on foam stability, using column experiments and Hele-Shaw cell experiments. The experiments performed in a horizontal Hele-Shaw cell provide information about foam coarsening in the absence of gravity drainage, while the column experiments allow quantifying the magnitude of gravitational drainage. In particular we present the first investigation of the synergy between non-ionic surfactant and nanoparticles.

Materials and Methods

Foaming suspensions:

All of the foam experiments were prepared using deionized water in ambient conditions (T~23˚C, RH~36%). We used deionized water to keep the chemistry as simple as possible although oil reservoir conditions could be saline. Three surfactants of different natures (respectively anionic, cationic, and non-ionic) were used in this study; sodium dodecyl sulfate (SDS) (Sigma, UK), dodecyl trimethyl ammonium bromide (DTAB) (Sigma, UK) and Triton X100 (Sigma, UK), respectively. The properties of these surfactants used in this work are summarised in Table 1. The surfactants were used at their CMC, (unless otherwise specified). Charge-stabilized dispersions of spherical colloidal silica particles~~Spherical charge-stabilized dispersions of colloidal silica particles~~ (Ludox HS, Grace) with a diameter of 16 nm were added to the surfactant solutions.

Table 1 Properties of the surfactants (Lin et al., 1999; Yu et al., 2012a), including the critical micellar concentration (CMC).

Surfactant	Charge	CMC (mM)	CMC (%w/w~~v~~)
Sodium dodecyl sulphate (SDS)	Anionic	8	0.23

Dodecyl trimethyl ammonium bromide (DTAB)	Cationic	11	0.46
Triton X100	Non-ionic	0.24	0.02

The interaction of the surfactants with the silica particles was characterized qualitatively using ultraviolet-visible (UV-vis) spectroscopy, with an analysis based on the method described by Desarnaud et al. (Desarnaud et al., 2016). It is based on measuring the decolourization ~~decolorization~~ of a dye solution (here a cationic dye: methylene blue (MB)) due to the adsorption of the dye on the oppositely charged surface (i.e., the silica particles). Here, one would expect that the formation of a silica-surfactant complex, due to charged interactions, would reduce the decolourization ~~decolorisation~~ of the MB solution due to the surface of the silica particles being essentially covered by adsorbed surfactant molecules, which limits absorption of the dye onto the particles' surface. To confirm this, silica particles were mixed in each of the prepared surfactant solutions. The solutions were then filtered and left to dry. The obtained dried particles were then placed in an MB solution, and using UV/Vis-spectrometer, the decolourization ~~decolorisation~~ of each dye solution was measured.

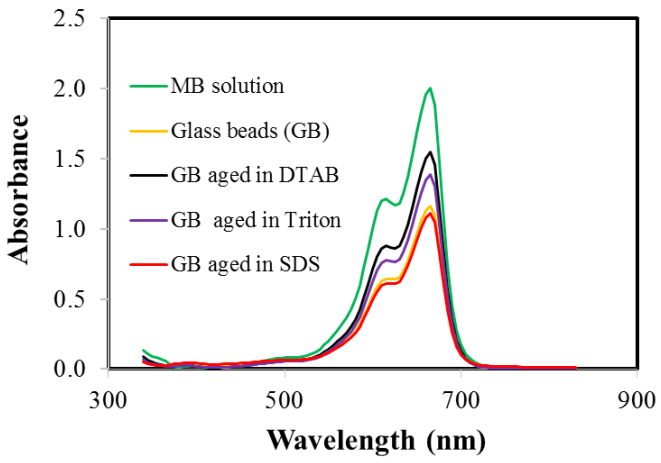

Figure 1: UV-vis absorption spectra of methylene blue solution (MB) after the addition of silica beads and silica beads treated in SDS, DTAB, and Triton X100 solution.

In the case of the negatively charged SDS surfactant, the measurements show that the anionic surfactant hardly adsorbs onto the negatively charged surface of the silica particles, presented in Figure 1, since the reduction of absorbance (indicative of the decolourization ~~decolorization~~ of the solution) is nearly identical when silica particles and silica particles treated in SDS solution are added to the methylene blue solution. ~~This observation is consistent with the recent work of Osman et al. (Osman et al., 2018).~~ Conversely, in the case of silica particles treated in DTAB solutions, the decolourization is measured to be significantly less intense due to adsorption of the cationic surfactants onto the oppositely charged silica surfaces, which minimize the interactions between the MB dye and silica. Similarly, but to a lesser extent, adsorption of Triton X100 onto the silica particles also occurs, as seen in Figure 1. Figure 13 in Appendix A shows an image of the solutions containing silica nanoparticles. In the case of DTAB (Figure 13b), flocculation occurs due to the strong interaction of the cationic surfactants with the anionic silica particles. The adsorption of DTAB onto the surface of the particles tunes the DLVO barrier, which describes the balance between charge-induced repulsive forces together with the attraction induced by van der Waals forces at a short-range (Derjaguin and Landau, 1993; Verwey and Overbeek, 1955). In this case, adsorption leads to a decrease in the electrostatic repulsion between the nanoparticles, and consequently, the van der Waals attraction become dominant, thus contributing to flocculation of the suspension.

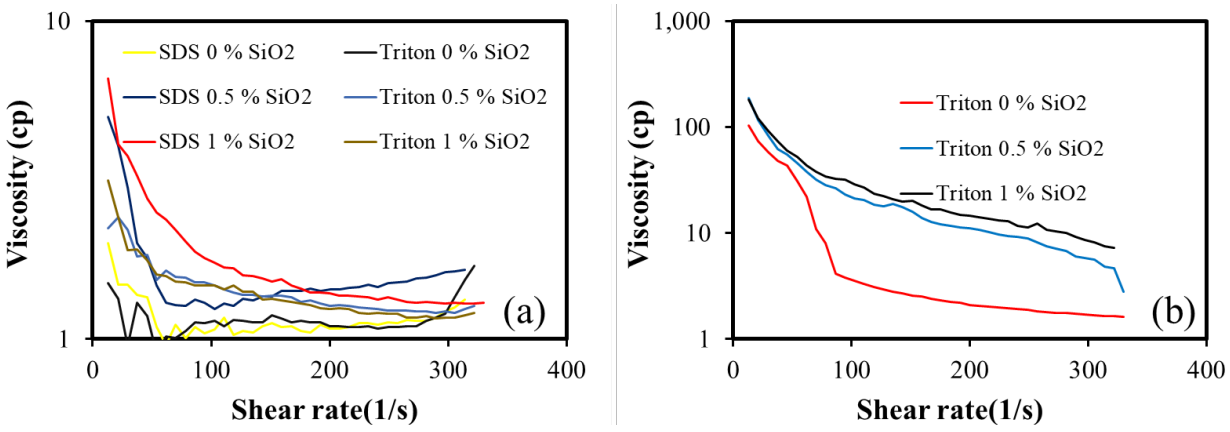

Figure 2: Dependence of the apparent viscosity on the shear rate of the different foaming suspensions at different silica nanoparticles concentrations. Both surfactants are at their CMC in (a). The concentration of Triton X100 in (b) is 1 % (is over 50 times CMC~~6.7 times more than its CMC~~). The vertical axis is in log scale. As the DTAB precipitated and we had two phases, we did not present its viscosity data in (a).

The rheology of the foaming suspensions was measured using a rheometer (Rotational DV3T Rheometer, Brookfield) in the plate-plate configuration. Figure 2 presents the viscosity's dependence on the shear rate for surfactant solutions at different nanoparticle concentrations for surfactants at the CMC (Figure 2a) and at 1% (Figure 2b). The plots do not exhibit monotonicity in shear rate as ~~expected~~, most probably due to heterogeneity in nanoparticle density within the samples during measurements. However, they show that the addition of silica nanoparticles tends to increase the viscosity of the solution: the larger the concentration in particles, the larger the viscosity. This effect is especially significant for Triton X100, as viscosity increases by up to one order of magnitude when particles are added for Triton at concentration of ~~was~~1%~~rather than~~as well as at~~This effect is especially significant for Triton X100, as viscosity increases by up to one order of magnitude when particles are added and surfactant concentration is increased from the CMC to 1 %~~. This ~~can~~ could be due to the interaction between nanoparticles and surfactants at high concentrations of Triton X100~~.~~ and also ~~probably~~ partly ~~due~~ to the fact that Triton X100 is a viscous liquid, which ~~would~~ explains the higher measured viscosities at low shear rates and 0wt% ~~NP~~nanoparticles. Note also that rheometry measurements could not be performed with DTAB together with nanoparticles, due to the flocculation of the nanoparticles in DTAB-based suspensions.

Experimental Set-up and Procedure

A series of foam stability experiments were conducted using a Hele-Shaw cell (Figure 3) and a column cell (Figure 3) to investigate the synergy between nanoparticles and surfactants in impacting foam stability at bubble and bulk-scale, respectively.

Bubble-scale experiments: The Hele-Shaw cell consisted of two plexiglass plates of dimensions 30 × 17 × 0.5 cm^3. The plexiglass plates were tightened using medium-duty clamps in all experiments. A gasket of thickness 1 mm was clamped between the two plates to impose a constant distance between them and prevent leakage. ~~Two~~ One hole~~s~~ (1 mm diameter) ~~were~~ was drilled on ~~opposite~~ the side~~s~~ on the top of the plexiglass plate to act as inlet ~~and outlet channels~~ for the flow of foam through the Hele-Shaw cell. Foam was generated by injecting both compressed air and the surfactant solution simultaneously into a foam generator fitted with a sintered glass disc (Scientific Glass, UK) with a pore size distribution between 40 and 60 µm. The flows of gas and surfactant were set to 10 ml/min and 1.11 ml/min respectively to achieve a 90 % foam quality for all the foam displacement experiments. The pressure was measured at the inlet of the Hele-Shaw cell via a pressure transducer, while the outlet was connected to the atmosphere. The Hele-Shaw cell was initially fully saturated by air.

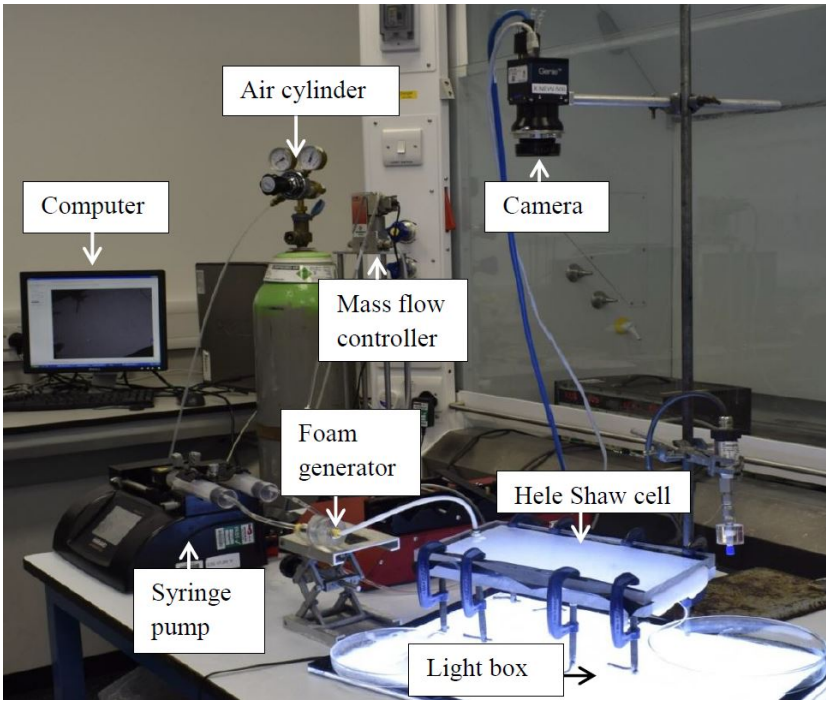

Figure 3: Hele-Shaw cell experimental set-up.

A high-resolution camera (Teledyne DALSA genie) was placed above the micro model and captured a snapshot of the ageing process every 30 minutes for a total of at 6 hrs or more. The images produced were 8-bit grey levels with a resolution of 2560 x 2048 pixels. The contrast of the images was improved by the use of a lightbox placed underneath the model.

The images were treated using ImageJ and Matlab in order to identify individual bubbles and measure their apparent area. The procedure is illustrated in Figure 4 using the image recorded 6.5 h after the start of the experiment performed with a suspension containing SDS at its CMC and 1% of SiO_2 nanoparticles. The raw image (Figure 4a) is first segmented using ImageJ's "local thresholding" procedure, with a local threshold value obtained from running a moving average filter with a window of linear size 500 pixels; the resulting image is shown in Figure 4b. From this image, a better image (Figure 4c) is obtained by removing all connected black regions except the largest one, which runs between the bubbles; this removes black spots which are seen inside bubbles in Figure 4b. Other black spots are removed from

bubbles in the image of Figure 4d, which has been obtained from that of Figure 4c by replacing each white connected region by its filled convex hull (that is, the filled convex polygon that covers the region the most closely). These two steps are done with custom-made MATLAB scripts. For some of the data sets this last step of the treatment is not necessary. Individual bubble areas are then measured from analysing the connected white regions in the image of Figure 4d, disregarding those of these regions which are in contact with an image boundary (and therefore, which correspond to bubbles that are not entirely captured inside the image). An outline of the corresponding bubbles is shown in Figure 4e.

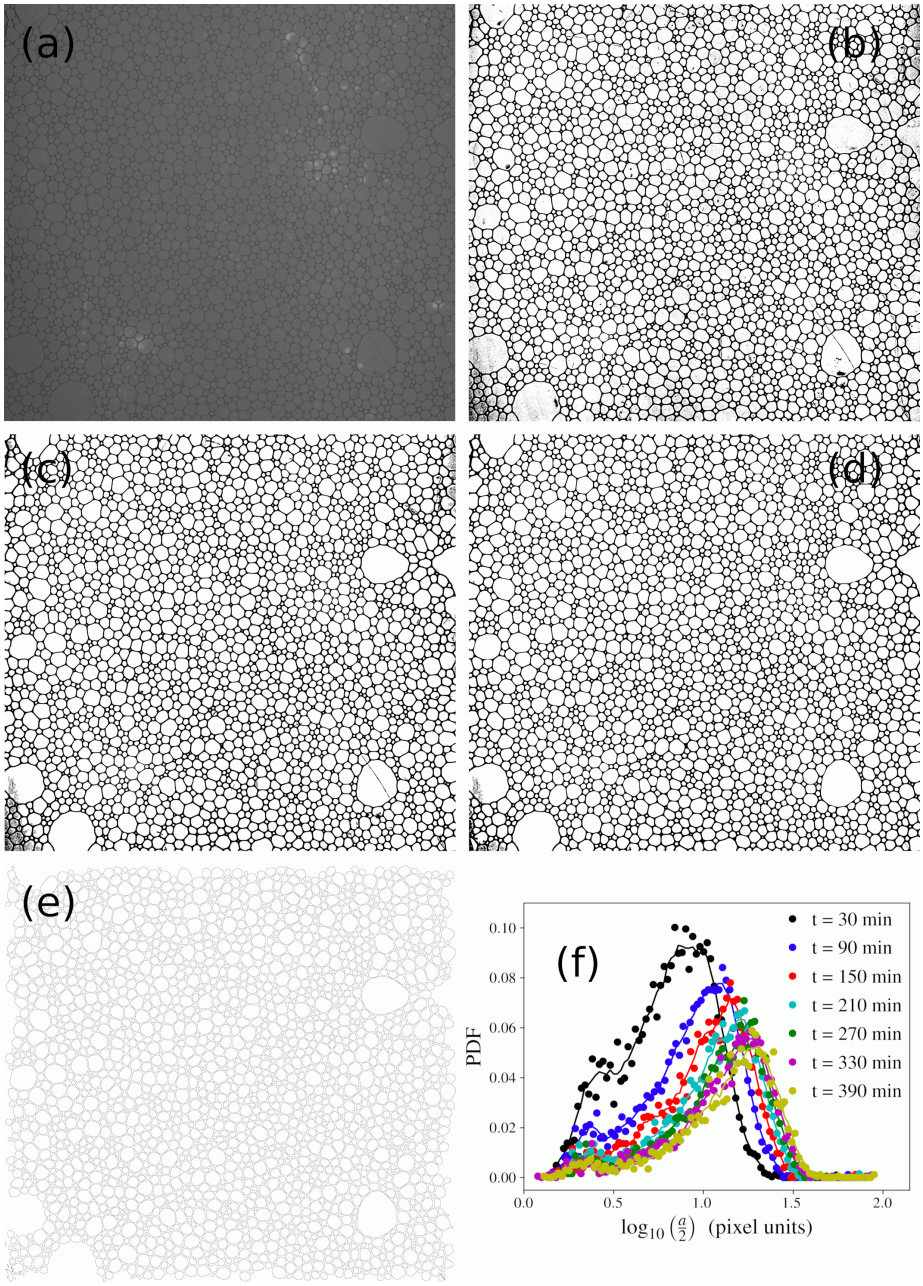

Figure 4: Various steps of the image treatment procedure: (a) Raw image; (b) Image segmented using the ImageJ "local thresholding" function based on local average; (c) image obtained from (b) by only keeping in the image the largest connected black region; (d) image obtained from (c) by replacing each connected white region by its filled complex hull; (e) Outlines of the resulted connected white regions which are identified as whole bubbles; (f) Corresponding temporal evolution of the PDF for the decimal logarithm of the equivalent radius, a/2 (equivalent particle diameter~~a being the equivalent particle size~~).

From the list of bubble areas, a list of equivalent radii is then obtained as the radii of the disks that have the same area as the bubbles. Statistical measures such as the mean and median values and the standard deviations are computed from these statistics, as well as the probability density functions of the equivalent radii, which is obtained from a histogram. Figure 4f shows the time evolution of the probability distribution function (PDF) of equivalent radii for the experimental run corresponding to Figure 4a-e. Note that since we consider the logarithm of the equivalent radius here, the distribution is becoming wider with time, and this to a considerable extent. The normalization of the PDF takes this into account, which is why its peak decreases with time. The visual impression that the area below the curves is not conserved with time is due to this log-binning of the equivalent radius. In fact, it is conserved, equal to unity at all times.

Bulk-scale experiments: The column experiments were conducted in a chromatography column (Scientific glass, UK) with an inner diameter of 4 cm and a height of 80 cm, respectively. Figure 5 shows a schematic diagram of the column used in this study. A sintered glass disc with a pore size distribution between 40 and 60 µm was placed at the bottom of the column as a foam generator. The liquid phase for each surfactant was prepared by adding the surfactants to deionized water at their CMC (Table 1) and then mixing using a stirrer (Fisher Scientific, UK) for 2 hours. Silica nanoparticles were added to the solution at various concentrations (0-1%) and mixed for an additional 30 minutes. The experiments were conducted immediately after the solution was prepared to prevent hydrolysis of the surfactants. Air was injected through a tube with an inner diameter of 0.5 cm into the column through the sintered glass using a mass flow controller at 100 ml/min flow rate. The gas flow rate was adjusted using the Flow View and Flow DDE (Bronkhorst, UK) software. Flow DDE ~~View~~ provides an interface between the computer and the mass flow controller while Flow ~~DDE~~ View provides the user with manual control of the desired flow rate. The injection

was stopped when the column had wholly filled with foam, that is when the foam inside the column had reached a height 80 cm. The liquid then drained from the column by gravity. The drained ~~mass of~~ liquid flowed to a reservoir placed on a balance and its mass was recorded ~~every minute for each experiment with a balance placed close to the column~~~~placed closely to the column~~at different times during each experiment. ~~The drained liquid transferred over the balance for the measurement.~~

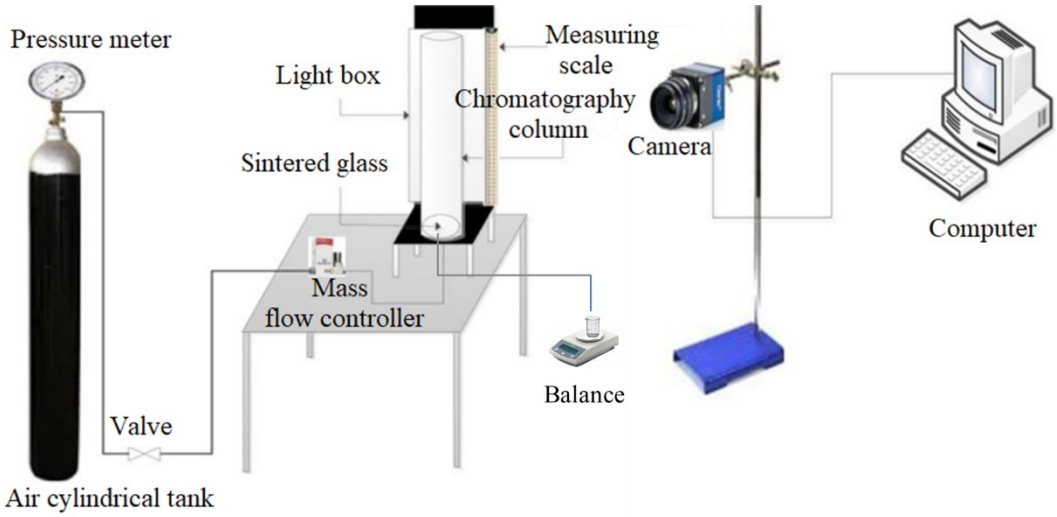

317

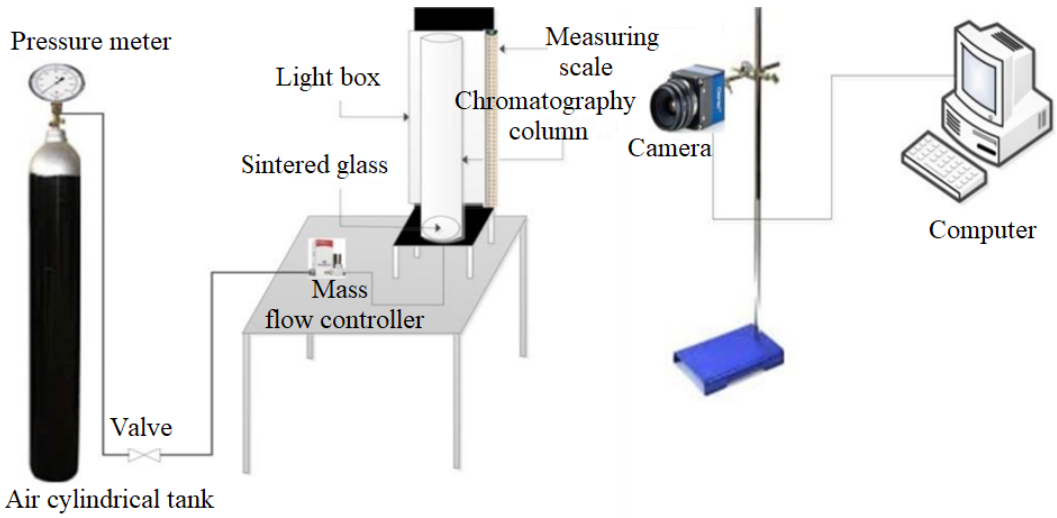

318

319 *Figure 5: A schematic diagram of the bulk-scale experiment set-up.*

320Each experiment was repeated three times to check the reproducibility. The results presented

321in the next section will thus be an average of all three tests unless specified otherwise. All ~~the~~

concentrations of surfactants and nanoparticles are percentage by weight ~~percent~~ (wt%), if not otherwise mentioned.

Results and discussion

Interaction between nanoparticles and surfactants affecting foam stability at bubble scale~~Synergistic effect of nanoparticles and surfactants on foam stability at bubble scale~~

A series of Hele-Shaw cell experiments were conducted to investigate the synergy between nanoparticles and surfactants in impacting foam properties at bubble scale. In these experiments, gravity-driven foam drainage was negligible since we were working with a quasi-two-dimensional model positioned horizontally.

Figure 6 shows the pressure drop measured during foam flooding of the Hele-Shaw cell at different experimental conditions. The pressure drop enables determining the apparent viscosity (Pa.s) of the foam based on the Darcy law: ~~(~~$\mu_{app} = \frac{KA}{q}\frac{\Delta P}{L}$, where K (m^2~~)~~) is the permeability of the Hele-Shaw cell, which is close to the theoretical value for infinite planes separated~~whis is close to the theoretical value for infinite planes distant~~ by e, $e^2/12$, e (m) being here the smallest dimension of the cell, q (m^3/s) is the flow rate, A (m^2) is the cross-sectional area, and L (m) is the length of the system). ~~As~~ The imposed flow rate (10 ml/min) and permeability are~~is~~ the same for all measurements~~here the imposed flow rate is the same for all measurements,~~. ~~w~~We use the pressure drop as a proxy for the apparent/effective viscosity of the foam~~. Hence the effective viscosity of foam is~~ since the two quantities only differ by a factor which is identical for all measurements ~~proportional to the pressure drop (all other things i.e. permeability, flow rate) being equal~~.

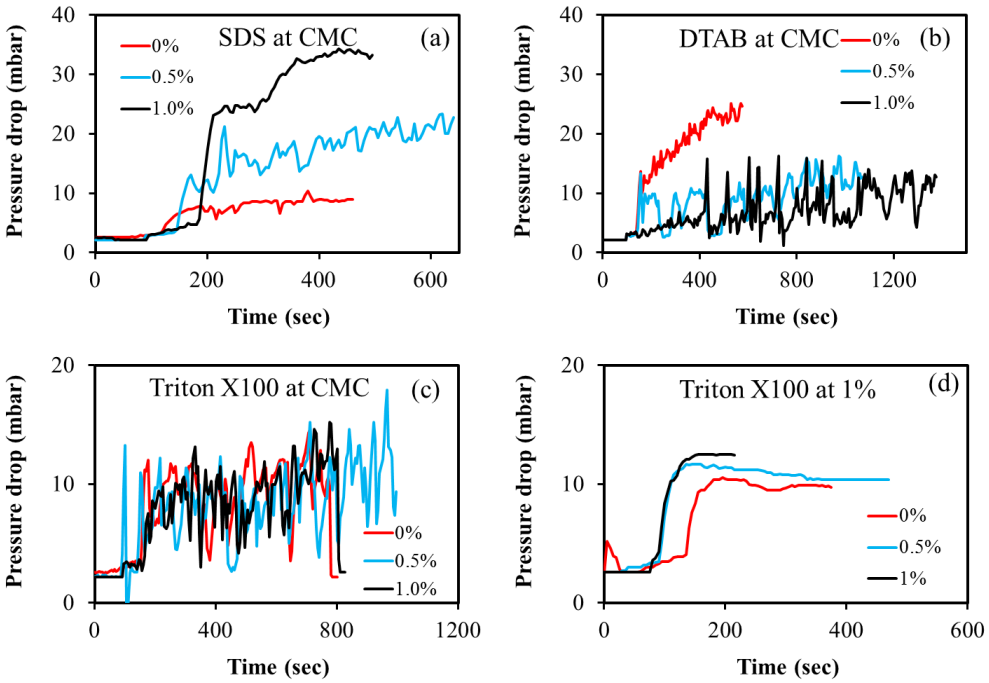

Figure 6: Measured pressure drop versus time during foam injection~~during foam injecting~~ at different experimental conditions in the Hele-Shaw cell. The legends indicate nanoparticle concentrations.

~~Figure 6 is already a surrogate for coalescence data. Systems that exhibit lots of coalescences tend to have unstable pressure drop signals. On the other hand, systems with limited coalescence have less noisy pressure signals that oscillate less.~~ Figure 6a shows the pressure drop for the SDS surfactant in the presence of silica nanoparticles. It can be seen that an increase in silica concentration leads to a larger pressure drop, which can be interpreted as the generation of a stronger foam. The presence of nanoparticles decreases the surface tension (Jia et al., 2020; Vatanparast et al., 2018) and increases the strength of the generated foam. In addition, Figure 6 also gives indication about the level of bubble bursting occurring in the foam. Given the simple geometry of the Hele-Shaw cell, pressure fluctuations are unlikely to be related to geometry-related capillary fluctuations, such as could occur inside complex porous media (Cox et al., 2004; Rossen, 1990). Unstable pressure drop signals are then likely

related to bursting events. Conversely, systems with limited bursting are expected to exhibit less “noisy” pressure signals, with less oscillations.

We stopped the injection of gas and liquid solution at the end of the experiments, and the structural evolution of foam bubbles was then monitored in time over the Hele-Shaw cell. Although these results were thereby obtained~~Although, these results were obtained~~ under~~at~~ static conditions, ~~but~~ they could~~an~~ be used as screening experiments prior to flow tests~~screening experiments for flow tests~~ (Jones et al., 2016; Nasr et al., 2019). Figure 7 qualitatively shows foam coarsening in the Hele-Shaw cell for eight different foaming suspensions, prepared with the three different types surfactants at a concentration equal to their CMC (and one surfactant well above CMC)~~for six different foaming suspensions, prepared with the three different types surfactants at a concentration equal to their CMC~~ and with two different concentrations of nanoparticles (0 and 1%). The pictures taken at time t=0 after the end of the injection show the foam structure at the end of foam generation while comparing the picture at t=0, and t=6 h provides information about foam coarsening. Comparing Figure 7a with Figure 7A~~g~~, show that the SDS foam has a finer texture in the presence of silica nanoparticles. ~~Although, t~~ The foam generator was ~~fixed, i.e. had fixed pore sizes~~the same for all generated foams (hence, with the same pore size distribution), but the bubble size/~~bubble~~ texture produced by a given generator (for specified gas and liquid flow rates) could vary from foaming suspension ~~liquid~~ to foaming suspension~~liquid~~. Indeed ~~the~~a finer texture foam could ~~relate to~~result from an increase in the maximum capillary pressure of coalescence due to the presence of silica nanoparticles, thereby leading to less film breakage during foam generation~~One reason for smaller bubbles mightcan be attributed to less film breakage that leads to smaller bubbles. Another possible reason for finer texture foam could be related to an increase in the maximum capillary pressure of coalescence due to the presence of silica nanoparticles leading to less film breakage~~. A finer textured foam ~~when~~

~~flowing~~ provides a higher pressure drop when flowing through a permeable medium, ~~A finer textured foam provides a higher pressure drop~~ and hence results in a higher apparent viscosity of the foam. ~~The other possible reason for finer texture foam could be related to an increase in the maximum capillary pressure of coalescence due to the presence of silica nanoparticles.~~

In the case of the DTAB surfactant, on the contrary, the presence of nanoparticles results ~~-~~in a decrease of the foam's apparent viscosity, as shown in Figure 6b. This is due, as ~~we have said~~discussed above, to~~This is due to~~ the adsorption of the cationic surfactants onto the silica nanoparticles, which promotes flocculation of the suspension, that is, phase separation of the solution between the flocculated/sedimented phase and the liquid phase, as seen in Figure 13b in the appendix. Consequently, less surfactant will be available in the solution for strong foam generation. Comparing Figure 7b with Figure 7~~h~~B shows coarser foam bubbles were generated in the presence of SiO_2. Higher fluctuation in pressure drop curves for a larger concentration of nanoparticles is also an indication of a more marked instability of the foam. This is due to ~~It could be due to the existence of a flocculated phase of colloids which does not easily contribute to foam formation when in contact with the surfactant solution and gas,~~the existence of a flocculated phase of colloids that sedimented out of the surfactant solution and did not enter the foam generator. This leads to~~that does not easily contact foam generator and leads to~~ low foam generation ~~does not occupy the volume of liquid phase homogeneously~~.

Figure 6c indicates that for Triton X100 at CMC Figure 6~~c~~ the foam is generally unstable both in the absence and presence of nanoparticles~~indicates that the foam is generally unstable in the absence and presence of nanoparticles for Triton X100~~, as indicated by the strong fluctuations, whose amplitude is not impacted by the concentration in SiO_2 nanoparticles. This might be due to the low molar concentration of Triton X100 at its CMC (Table 1). Generation of even a limited amount of foam can then reduce the concentration in the bulk

solution below the CMC, which can affect ongoing foam generation (Boos et al., 2012). This effect can be intensified in the presence of nanoparticles given the low ~~CMC value~~molar concentration of Triton X100 at the CMC (see Table 1). ~~The issue is that the CMC corresponds to a low molar concentration and mass concentration (compared to the other surfactant),~~ meaning that ~~``~~"losing" a given mass of Triton to adsorption on the particles, can significantly impact ~~a great deal on~~significantly the concentration remaining in the bulk solution. ~~To validate this point, we performed experiments at a higher concentration (1.0 %) of Triton X100 with varying concentrations of silica nanoparticle~~Consequently, ~~s~~w~~W~~e also performed experiments at a higher concentration (1.0 %) of Triton X100 with varying concentrations of silica nanoparticles to investigate the impact of the concentration of Triton on the foam's stability~~validate this point~~. The corresponding temporal evolution of the pressure drop across the flow cell is presented in Figure 6d. Comparisons between Figure 6c and Figure 6d, with the plots in Figure 6d appearing much smoother than those in Figure 6c, shows that an increase in the surfactant concentration improved foam stability~~shows that an increase in the surfactant~~ concentration improved foam stability tremendously. These findings suggest that surface tension (which tends to remain fixed above the CMC) is not the only physical quantity- controlling foam stability and foam generation and that CMC may not be the optimal concentration to generate the most stable foams in the case of surfactants with an extremely low CMC, in particular in the case of attractive interaction between the nanoparticles and the surfactant. Note also that once the quantity of surfactant available for the fluid-gas interfaces is sufficiently large (Figure 6d), the addition of SiO_2 nanoparticles slightly enhances the foam's apparent viscosity, but to a significantly lesser extent than what is observed in Figure 6a for the SDS-based foaming solutions.

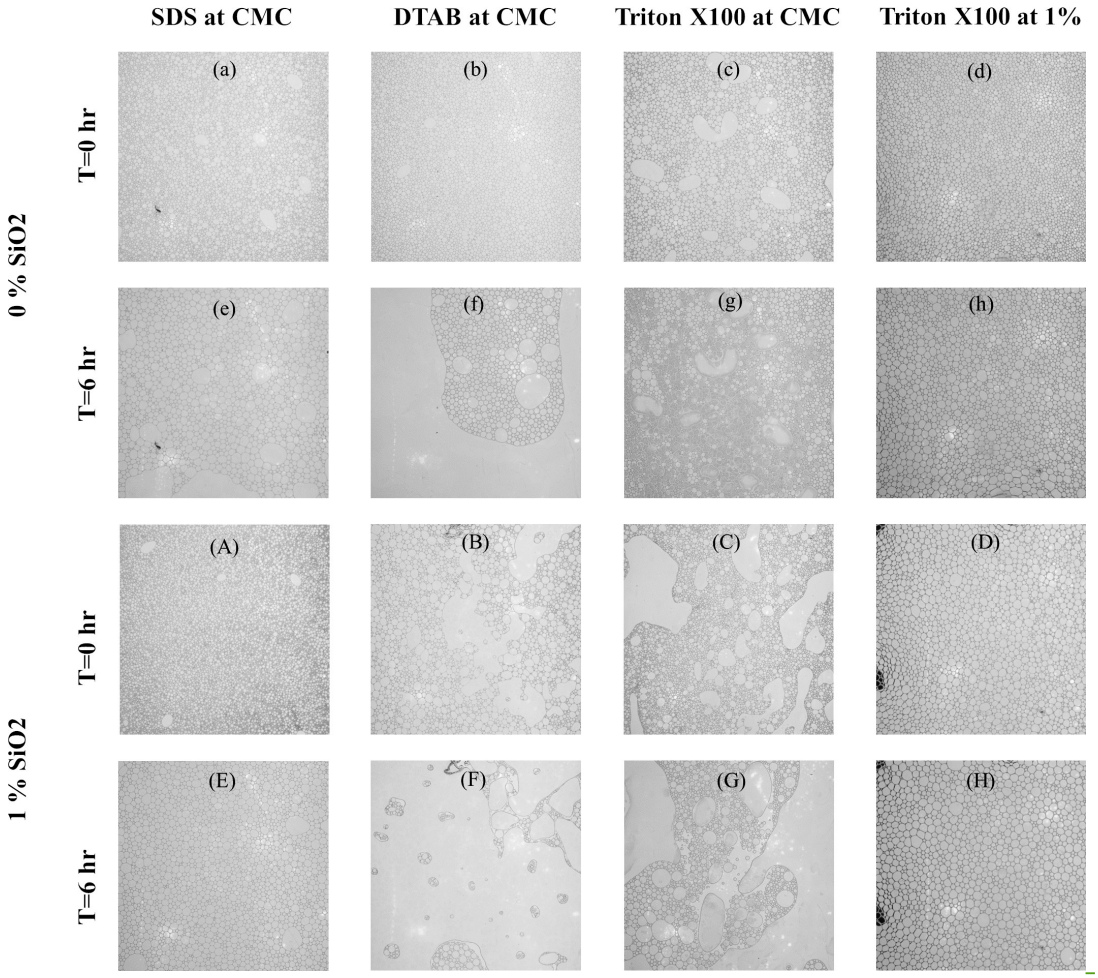

431

432*Figure 7: Bubbles observed for different foaming suspensions~~observed for six different~~*

433*~~foaming suspensions~~, corresponding to the three types of surfactants and two different SiO_2*

434*concentrations of 0 and 1%, at two successive times 0 hr and 6 hr after the flow has been*

435*stopped in the Hele-Shaw cell. ~~All surfactants are at a concentration equal to their CMC.~~*

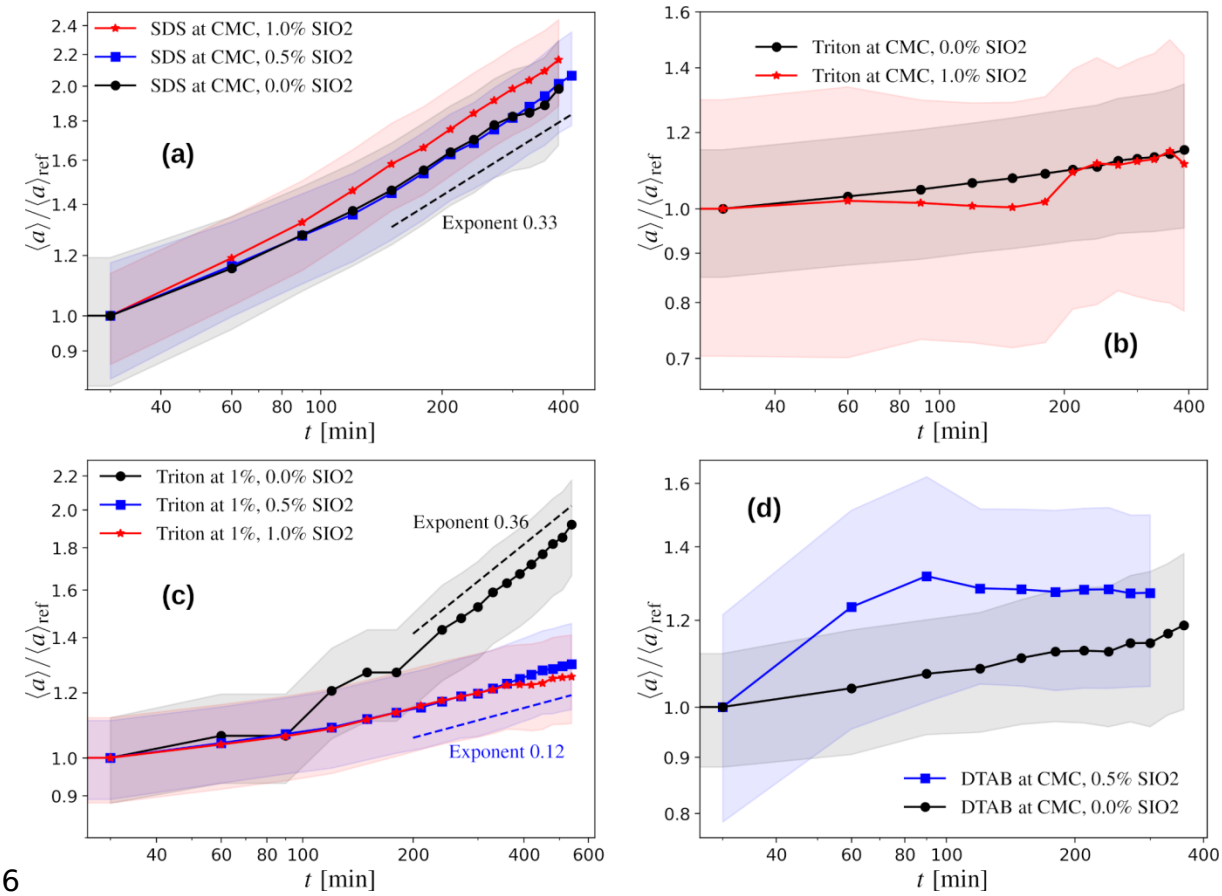

436

437*Figure 8: Ratio of the mean ~~initial~~ equivalent bubble radius,* $\langle a \rangle / 2$*, to its value at time* $t = 30$

438*min, plotted as a function of time for different foaming suspensions prepared with the three*

439*types of surfactant and different concentrations of* SiO_2 *nanoparticles, as presented in the*

440*legends. Each coloured area corresponds to the tolerance interval of the curve of identical*

441*colour, defined as having a vertical extent equal to half the standard deviation of* $\langle a \rangle / \langle a \rangle_{ref}$.

442Image analysis performed from images such as presented in Figure 7 allowed us to extract the

443probability density functions (PDFs) of bubble sizes, as explained in the “Methods” section

444above. ~~-~~Figure 8 summarizes the behaviour observed for the mean ~~and standard deviations of~~

445these PDFs, for four types of foaming solutions and, depending on the case

446considered~~depending on the foaming solution, for two or three concentrations of the~~

447~~nanoparticles.~~ ~~definition~~, for two or three concentrations of the nanoparticles. This quantity

448is ~~mainly~~a measure of ~~(likely to be associated with~~ bubble coarsening by both gas diffusion

and film breakage insofar as the latter results in a coalescence of two bubbles into a larger one. Bubble bursting would be expected to lead to size distributions where a few larger bubbles exist in the midst of smaller bubbles (see for example *Figure 7c* and *7g*), but distinguishing between coarsening by gas diffusion and by film breakage was made difficult by the initial polydispersity of the foams. Note also that in our image treatment (see *Figure 4*), the bubbles that touch the boundaries of the field of view are not taken into account in the statistics, because their real size may not be (and in most cases, is not) captured entirely in our image. For the DTAB-based foams and those based on Triton at CMC, the foam is observed to burst over large areas starting from the boundaries of the domain until a large part of the domain corresponds to the result of that "catastrophic" bursting (see *Figure 6f*, *6F*, *6g* and *6G*). The measure of the mean bubble size is insensitive to large scale bubble bursting ~~is blind to they may include some bubble coalescence. However, large-scale this large scale bubble bursting~~ since~~is not included in this~~ large boundary-touching voids are excluded from the calculation~~calculation~~. The total number of bubbles N~~The total number of bubbles~~ measured by the image treatment, on the contrary, decreases strongly due to that large scale bursting. For foams in which no such catastrophic bursting is visible, the squared mean bubble size $\langle \rangle^{\square}$ (which does not differ much from $\langle \square^{\square} \rangle$) and the inverse number of bubbles, when normalized by their initial value, are supposed to be more or less equal to each other since the sum of all bubble areas is not very different from the total domain area. Indeed, *Figure 9* confirms a linear relationship between the two quantities for the SDS-based foams and the foams based on Triton at 1%. The slope is not exactly 1, probably because the apparent area of the lamellae has been neglected in the above argument, but one can safely conclude that, for these foams, the two quantities (mean bubble size and number of bubbles) contain the same information. For foams based on Triton at CMC with nanoparticles and those based on DTAB, on the contrary, the information on the mean bubble size and standard

deviation of the bubble size PDFs is not conclusive without additional information on the number of bubbles.

~~coalescence may be going on also, but t~~Note also that too a certain extent, the pressure fluctuations in Figure 6 are ~~already a~~indicative of large scale bursting ~~proxy measurement for it,~~ which complement the present~~so we look instead at diffusive coarsening in what follows~~ measurement of bubble coarsening.

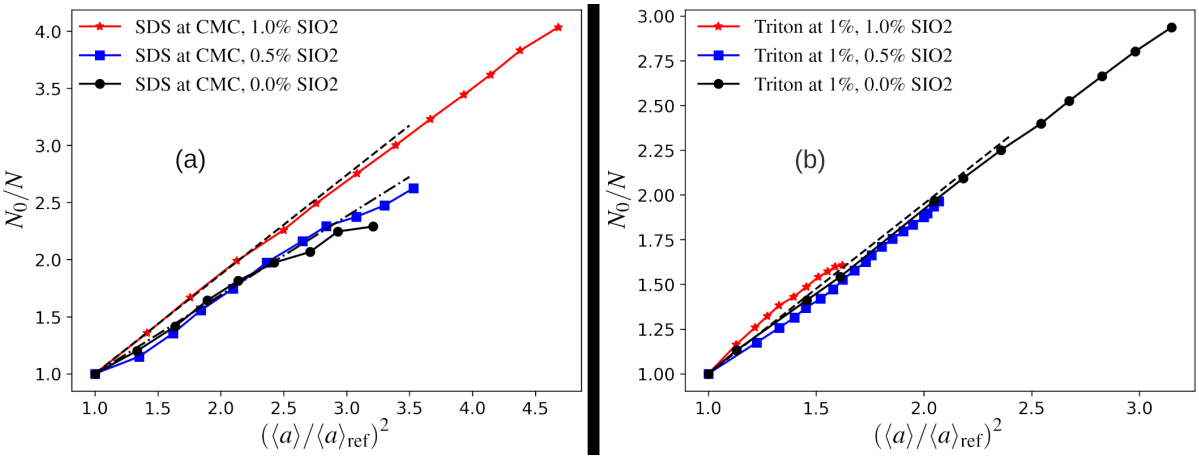

Figure 9: Relationship between N_0/N (N_0 being the number of bubbles at t=30 min) and $\langle\rangle$ normalized by its value at t=30 min, for (a) SDS-based foaming suspensions, and (b) foaming suspensions based on Triton at 1%.

Returning to consider Figure 8a, this presents the resultsFigure 8~~a presents the results~~ for a foaming solution consisting of SDS at the critical micelle concentration (CMC). For the three nanoparticle concentrations (0.0, 0.5 and 1.0%), the evolution in time of the bubbles' mean radius $\langle a\rangle/2$, recorded over a duration of about 400 min and normalized by its value at t=30 min, shows that all three curves tend to follow power laws of exponent 0.33 after t=150 min, but with a prefactor which is about 10% larger for the largest concentration in SiO_2. The dispersion of the PDF around the mean follows a similar behaviour, proportional to the mean.

This seems to indicate that adding nanoparticles at these concentrations does not provide any limiting effect on foam coarsening for SDS-based foams.

In the case of Triton X100, Figure 8b and Figure 8c reveal that a change in the concentration of the surfactants can radically modify their impact on foam coarsening and coalescence.~~their impact on foam coarsening.~~ This can clearly be associated with the combined effects of the extremely low CMC value of Triton X100 and of its interaction with the silica nanoparticles in line with the result of another study (Martinez et al., 2008). Indeed, at low concentration of Triton X100, ~~most~~ much of the surfactant adsorbs~~of the surfactants adsorb~~ onto the surface of the silica particles, leaving little surfactant deposition at the gas-liquid interface. This is detrimental to foam stability and foam generation, as discussed above in relation to Figure 6 and Figure 7. T~~Note however t~~he mean bubble radius evolves in a similar manner in the absence of SiO_2 nanoparticles as in their presence at 1.0% for Triton X100 at CMC, though the visual observation of the two bubble populations shows two very different behaviours: in the presence of the nanoparticles, the aforementioned ~~many bubbles burst, leading to the appearance of liquid films on the horizontal glass plates, which hide part of the bubbles population on the image~~large scale bursting from the domain boundaries occurs; on the contrary, in the absence of nanoparticles, the bubbles evolve through diffusion-controlled coarsening, with bubble sizes evolving in time but few of them bursting within the experimental time duration. Figure 9(b) ~~simply means~~confirms, as discussed above, that the mean bubble size of surviving bubbles is not, when comparing these cases, a good measure of the foam stability when large scale bursting occurs. Accordingly, the N_0/N plots (not shown here), show a much steeper increase in the presence of SiO_2 nanoparticles, as a consequence of the large scale bursting, than in the absence of SiO_2. We can conclude from this data that the affinity of Triton with the nanoparticles renders its use at CMC ineffective to study the

impact of added nanoparticles on the foam's stability. ~~It worth mentioning, Figure 8 focusespresents diffusive coarsening behaviour (not coalescence) on the diffusive coarsening behaviour, because of the particular way we defined the bubble radius <a>/2 (i.e. deliberately omitting large voids), what we are presenting with Figure 8 is the diffusive coarsening (not coalescence) behaviour. Regarding presenting foam coalescence, Figure 6 already gives a ``surrogate'' for coalescence data. Systems that exhibit lots of coalescences tend to have unstable pressure drop signals. On the other hand, systems with limited coalescence have less noisy pressure signals that oscillate less, and we highlighted this point in the manuscript.~~

For Triton X100 at 1%, on the contrary, there is enough surfactant for it to be present at liquid-gas interfaces while also adsorbing onto the nanoparticles, as discussed above in relation to Figure 6c and Figure 6d. Foam coarsening is then observed to be strongly impacted by the addition of SiO_2 nanoparticles. Coarsening of the foam prepared with the suspension devoid of nanoparticles exhibits a power-law growth of the mean bubble size, of exponent 0.36. If nanoparticles are added to the foaming suspensions, this power-law behaviour has an exponent 0.12, which is identical for concentrations of 0.5% and 1.0%in SiO_2. This is consistent with the observations of Figure 6d, showing that the foam's effective viscosity is larger as the concentration in SiO_2 nanoparticles is larger. However, the impact on foam stability ~~against~~of diffusive coarsening and bubble coalescence over time~~However,~~ ~~the impact on foam stability over time~~, demonstrated here, is more spectacular than the impact on its effective viscosity.

In contrast, according to Figure 8d, foam coarsening becomes faster in DTAB-based suspensions as the concentration in silica nanoparticles is larger. This is likely due to the interaction between DTAB and SiO_2, which results in flocculation of the suspensions, and therefore in a decrease of the number of nanoparticles available for the liquid-gas interfaces, as discussed earlier. The curve for 0.5~~1~~% SiO_2 shows a fast initial increase of the mean

bubble size, followed by a plateau. This plateau is somewhat misleading as it results from the disappearance of larger bubbles by bursting, which leaves only smaller bubbles whose size does not~~n't~~ evolve much to contribute to the mean bubble size. This is confirmed by the time evolution of the normalized inverse number of bubbles, N_0/N (Figure 10), in which the initial rise is much steeper than for the foam prepared without SiO_2 nanoparticles, but soon reached a plateau. This corresponds to extremely fast catastrophic bursting from the boundaries, leading to a configuration where the bubbles left are essentially round and isolated (which removes the possibility of coarsening by gas diffusion~~This plateau value in~~ Figure 8~~d~~); the bubble number then slowly evolves under additional slow bursting of these isolated bubbles, which explains the plateau in Figure 10, but bubble sizes hardly change any more, which explains the plateau value in Figure 8d. This plateau ~~is,~~ however, corresponds to a bubble size larger than the mean bubble size measured during the evolution of the foam which is devoid of SiO_2 particles. In a 2-d Hele-Shaw cell geometry, as gas escapes from (but liquid is retained by) a foam that is no longer connected to the cell walls, thus the effective liquid fraction of the foam rises over time, and diffusive coarsening is expected to slow as a result (Furuta et al., 2016).

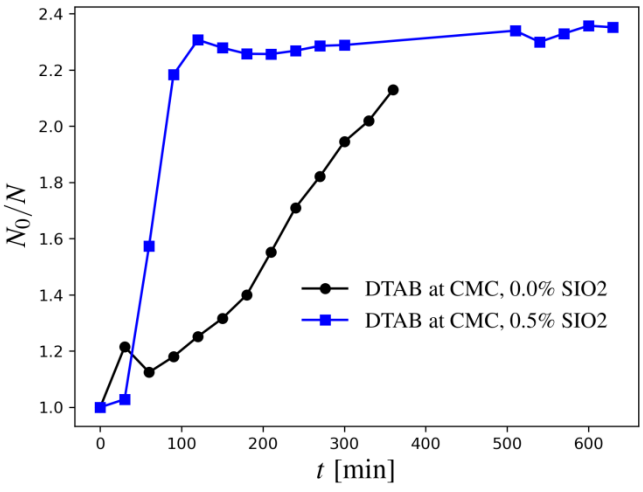

Figure 10: Time evolution of the ratio of the initial number of bubbles to the current one, for the foams prepared with DTAB at CMC.

In *Figure 11* we have plotted the time evolution of the mean bubble radius for SDS and Triton-based foams, grouping in *Figure 11**a*** all the data obtained with foams devoid of SiO_2 nanoparticles, and in *Figure 11**b*** all the data obtained with foaming solutions containing the nanoparticles at a 1.0% concentration in weight. *Figure 11a~~a~~* shows that, in the absence of SiO_2 particles, the foams prepared with SDS at CMC and Triton at 1.0% behave in the same manner, while that prepared with Triton at CMC ages more slowly. When SiO_2 nanoparticles are present at a concentration of 1% in weight, the aging of the foams based on SDS ~~and Triton at CMC are not~~ is not much impacted, while that of the foam prepared with Triton at 1% is slowed down considerably. For Triton at CMC, the mean bubble size does not vary much, but ~~the~~ the discussion above has shown that ~~that it is actually an artefact of the measure used to characterize bubble size during ageing, since bubble bursting is not accounted for~~this quantity is simply not a relevant measure of foam aging in this configuration, since the number of bubbles decreases dramatically due to large scale bubble bursting. F~~However, f~~or a sufficiently large concentration of Triton (such as 1%wt), however, the addition of nanoparticles improves the foam stability, while it has little impact on an SDS-based foam. Recall that adding nanoparticles to a 1% Triton solution led to a large increase in viscosity (see Figure 2). This is expected to reduce gas diffusivity through films (hence reducing diffusive coarsening) and also to reduce the rate at which films break (hence reducing coalescence). This may explain the slower coarsening seen when nanoparticles are added to 1% Triton solution.

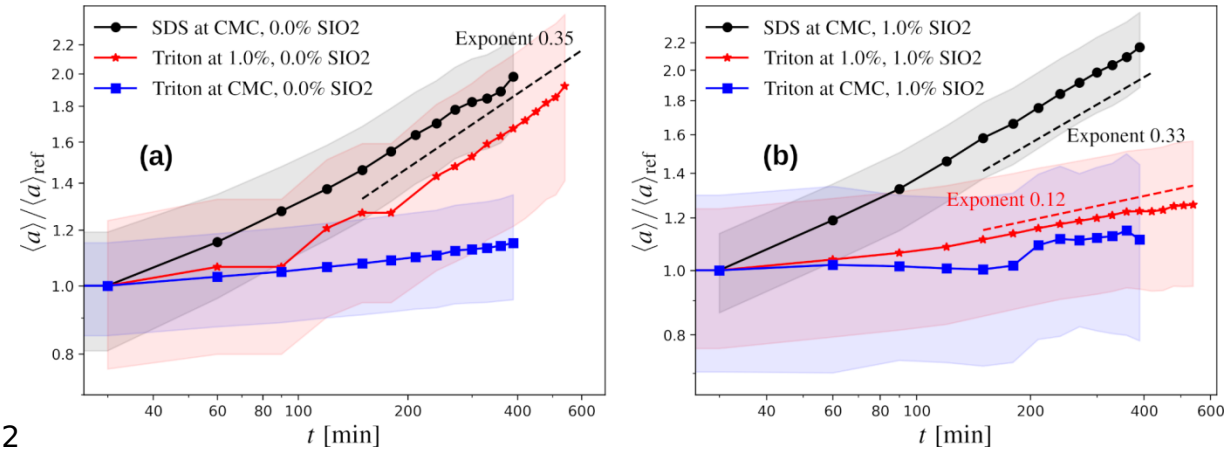

Figure 11: Ratio of the mean initial equivalent bubble radius, $\langle a \rangle / 2$, to its value at time $t = 30$ min, plotted as a function of time for different foaming suspensions prepared with the three types of surfactant and either 0% (a), or 1% (b) of SiO_2 nanoparticles, as presented in the legends. Each coloured area corresponds to the tolerance interval of the curve of identical colour, defined as having a vertical extent equal to half the standard deviation of $\langle a \rangle / \langle a \rangle_{ref}$.

Interaction between nanoparticles and surfactants affecting liquid drainage~~Synergistic impact of Nanoparticles and Surfactants on Liquid Drainage~~

The duration of the column experiments is between 15 min and 1hr (see Figure 12Figure 12). This duration is nearly one order of magnitude smaller than the time scales which are characteristic of foam coarsening, as probed by the Hele-Shaw experiments. Hence the column experiments investigate mostly the effect of gravitational drainage on foam stability, rather than that of~~and not~~ diffusive coarsening and bubble coalescence~~Hence the column experiments investigate mostly the effect of gravitational drainage on foam stability~~.

Figure 12 Figure 12 presents the mass of drained liquid measured at the bottom of the column for 11 different foaming suspensions. The end of the experiments was~~ere~~ defined~~termined~~ at the state when either ~~there was~~ no further change in the liquid drainage was visible, or all the foam bubbles inside the column had collapsed. Typically the former situation was observed

with experiments corresponding to Figure12s ~~(~~a~~)~~, ~~(1~~012b~~)~~, ~~1~~012~~and (~~d, whereas~~)~~ ~~and~~ the latter situation was observed with experiments corresponding to Figure12c.

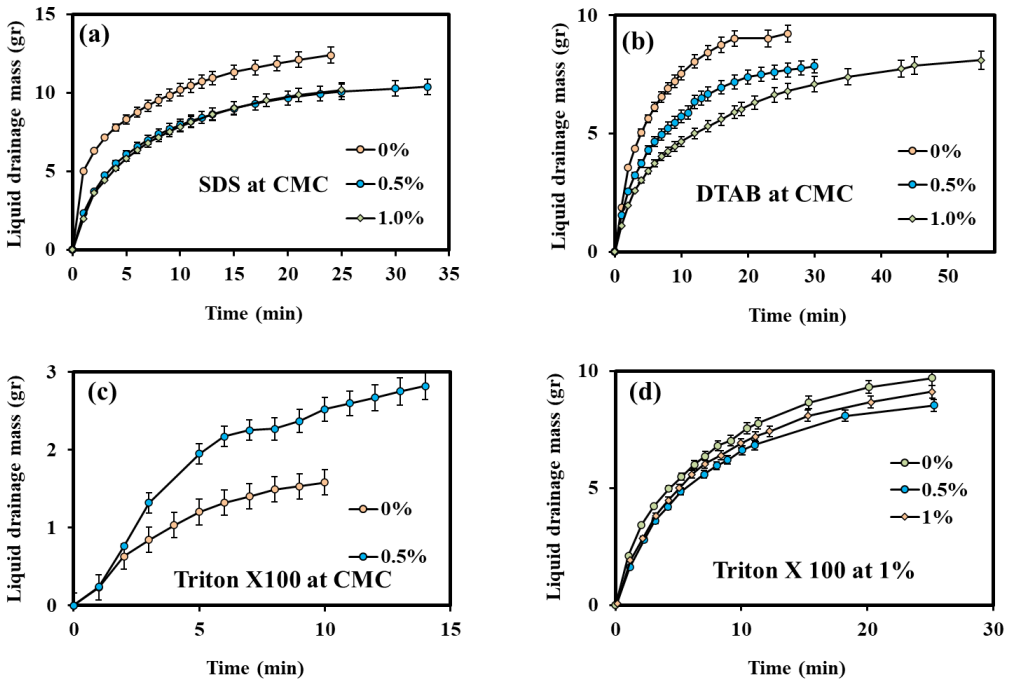

Figure 12: Liquid drainage over time for different foaming solutions based on SDS, DTAB, and Triton X100 surfactants (the latter at two different concentrations). The legends indicate nanoparticles concentration. Foam generation did not occur for Triton X100 at its CMC and 1 % concentration of SiO_2.

Figure 12Figure 12 a for SDS shows that the drained liquid mass at any given time decreases with the addition of the SiO_2 nanoparticles at 0.5 wt% compared to the same surfactant solution devoid of nanoparticles. This is probably due in part to the increase in the solution's viscosity resulting from the presence of the nanoparticles. However, a further increase in nanoparticle concentration from 0.5 to 1% results in no significant changes in the liquid drainage rate: the effect saturates. This indicates that the slower drainage is also related to the occupation of the gas-liquid interfaces by the nanoparticles, an effect that is likely to saturate at sufficiently high ~~enough~~ concentration of NPs. Covering interfaces with NPs

decreases their surface tension~~This indicates that the slower drainage is also related to the occupation of the gas-liquid interfaces by the nanoparticles, which decreases the surface tension~~ (Jia et al., 2020; Vatanparast et al., 2018) thus rendering them more stable and delaying their bursting due to lamella-thinning. Another possible reason for stabilising behaviour is that the nanoparticles can also slow the drainage down by ~~blocking~~rendering the Plateau borders less permeable to liquid~~renderingles permeable~~ (Carn et al., 2009).

In the case of DTAB, addition of the nanoparticles lowers the rate of liquid drainage significantly, and liquid drainage becomes slower as the concentration in silica nanoparticles is larger (see *Figure 12Figure 12 12*b). This is believed to be due ultimately to the adsorption of DTAB~~This is due to the adsorption of DTAB~~ surfactants on the silica particles, as shown in *Figure 1*, which leads to a decrease in the electrostatic repulsion between the nanoparticles, and thus to flocculation, as discussed earlier. Hence, after the solution was poured into the column, the particle-surfactant complex precipitated at the bottom of the column on the foam generator. This interaction between DTAB and silica nanoparticle increases the viscosity of the complex fluid considerably. This flocculated part of the mixture contributes to the largest part of the foam generation since it is where air first contacts the solution. This highly viscous solution present in the lamellae and Plateau borders decelerates liquid drainage.

In the case of Triton X100, Figure 12*Figure 12*c and *Figure 12Figure12* d suggest that the effectiveness of silica nanoparticles to generate foams which are less prone to collapsing under gravitational drainage depends on the concentration of the surfactant, as was the case for the Hele-Shaw cell experiments. Figure 12Figure12c for Triton at CMC shows that the drained liquid mass measured at any given time increases with the concentration of nanoparticles. For the 1% SiO_2 concentration, foam generation hardly occurred due to adsorption of ~~most~~ much of the surfactant of the nanoparticles, as discussed at length above in relation to Figures 6, 7, and 8~~ and 9~~; hence we have not included the corresponding data in

*Figure 12*Figure12c. At a concentration of Triton X100 of 1%, *Figure 12*Figure12d suggests that a 0.5% concentration in nanoparticles provide higher stability against gravitational drainage than 0 and 1% concentrations. This means that a further increase in silica nanoparticle concentration from 0.5% led to faster liquid drainage, possibly due to a saturation of the effect related to occupation of liquid-gas interfaces by nanoparticles. Note that in the case of ~~Interestingly foam is found to have a higher drainage rate with a higher concentration of~~ Triton X 100~~s~~ at CMC (c~~C~~~~omparing~~ Figure12 ~~(~~c), comparatively little drains out ~~with (d))~~ because the initial volume of generated foam is far from reaching the entire volume of the cylindrical cell unlike the other cases.~~at the higher concentration was much larger than the lower concentration. In other words, despite its high viscosity, Triton drains faster at a higher concentration as we already explained compared to Triton at CMC and more liquid enters to the foam network in the first place. Hence, as Triton at CMC forms a relatively small amount of~~little foam, there is relatively little liquid to drain out of the foam.

Summary and conclusion

We have presented an investigation of foam stability using surfactants with different charges (anionic, cationic and non-ionic) in the presence of charge-stabilized silica (SiO_2) nanoparticles. A comprehensive series of experiments were conducted using a horizontal Hele-Shaw cell and columnar flow cells. Hele-Shaw cell experiments are typically termed 'bubble scale' experiments in the literature (Osei-Bonsu et al., 2016); in our study, they mostly probed the foam's instability by coarsening through gas diffusion or ~~else~~ by bubble bursting~~instability by coarsening through gas diffusion and bubble bursting~~. Columns experiments are typically termed 'bulk scale' experiments; more importantly, they mostly probe the foam instability by gravitational drainage.

For foams prepared with the anionic surfactants SDS (which do not adsorb on SiO_2 nanoparticles), the presence of the nanoparticles increased foam stability with respect to

foam apparent viscosity (i.e., measured pressure drop during flow) and with respect to gravitational drainage but had little impact on foam coarsening by diffusion. In the case of a foaming suspension prepared with the cationic surfactant DTAB, the presence of oppositely charged nanoparticles leads to flocculation and sedimentation of the nanoparticles, which removes surfactant adsorbed on the particles from the solution. Consequently, the foam is less stable, ~~both in terms of gravitational drainage in the columns and~~ at least in terms of coarsening in the Hele-Shaw cells. Apparent viscosity, ~~i.e.~~which is inferred from the measured pressure drop signal during flow through the Hele-Shaw cells, also fluctuates a great deal for DTAB with nanoparticles, suggesting poor foam stability ~~in terms of coarsening in the Hele-Shaw cells~~.

For foaming suspensions prepared with the surfactant Triton X100, which adsorbs on the SiO_2 nanoparticles but to a lesser extent than DTAB, the concentration in surfactant should significantly exceed the CMC so that enough surfactant is present at the liquid-gas interfaces to generate stable foam. Of course, the amount of surfactant needed depends on the concentration of nanoparticles. Once this requirement is met, our findings suggest that there exists a concentration of nanoparticles that allows slowing down gravitational drainage optimally, whereas the addition of even more nanoparticles is all the more beneficial in terms of limiting foam coarsening by diffusion when the concentration in nanoparticles is larger. Therefore, finding the formulation of the foaming suspension, which is optimal in terms of global stability of the foam is not straightforward. Compatibility experiments between surfactant and nanoparticles are pre-requisite to optimizing foam stability.

The prospects of this study include similar experiments performed within porous media. In addition, since in deep geological formation solutions are often strongly ~~alkaline~~saline, one can wonder how these results would be impacted when considering foaming suspensions in saline solutions. An increase in salt concentration will shrink the electrical double layer's

thickness and thus favour nanoparticle attractive interactions and flocculation. Hence, the balance between the various forces at play will be displaced when increasing the salt concentration, but we expect most of the phenomenology to be similar. We shall test these hypotheses on the effect of salinity in future studies, as well as investigate the impact of high temperatures.

Acknowledgements

We would like to acknowledge the UK Engineering and Physical Sciences Research Council (EPSRC) for providing the Ph.D. studentship for Mohammad Javad Shojaei. All the experiments related to the analysis of foam stability at the bubble- and bulk-scale were conducted at The University of Manchester. The authors are grateful to Dr. Sajad Kiani for conducting rheology measurements.

-

Appendix A: Visual aspect of the various foaming solutions with nanoparticles

Three bottles containing foaming suspensions consisting of SiO_2 nanoparticles at 1% by weight suspended in solutions of the surfactants Triton, DTAB and SDS, respectively, are shown in *Figure 13.*

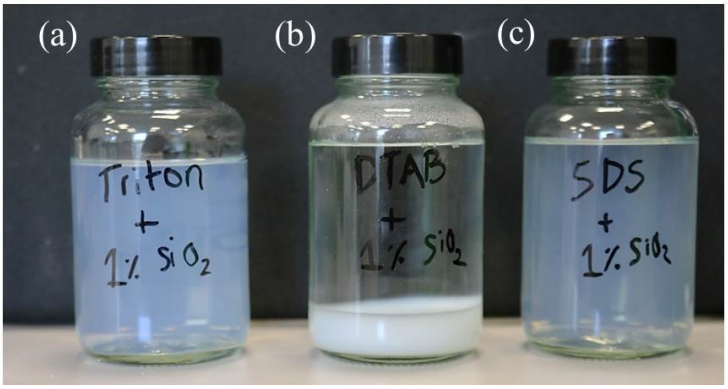

Figure 13: Visual aspect of surfactant solutions (a) Triton X100 (b) DTAB and (c) SDS containing silica particles (1%).

References

~~Uncategorized References~~

AttarHamed, F., Zoveidavianpoor, M., Jalilavi, M., 2014. The incorporation of silica nanoparticle and alpha olefin sulphonate in aqueous CO2 foam: Investigation of foaming behavior and synergistic effect. Petroleum science and technology 32, 2549-2558.

Benson, S.M., Cole, D.R., 2008. CO2 sequestration in deep sedimentary formations. Elements 4, 325-331.

Bhakta, A., Ruckenstein, E., 1997. Decay of standing foams: drainage, coalescence and collapse. Advances in Colloid and Interface Science 70, 1-124.

Bi, Z., Liao, W., Qi, L., 2004. Wettability alteration by CTAB adsorption at surfaces of SiO2 film or silica gel powder and mimic oil recovery. Applied Surface Science 221, 25-31.

Blijdenstein, T., De Groot, P., Stoyanov, S., 2010. On the link between foam coarsening and surface rheology: why hydrophobins are so different. Soft Matter 6, 1799-1808.

Blunt, M., Fayers, F.J., Orr Jr, F.M., 1993. Carbon dioxide in enhanced oil recovery. Energy Conversion and Management 34, 1197-1204.

Boos, J., Drenckhan, W., Stubenrauch, C., 2012. On how surfactant depletion during foam generation influences foam properties. Langmuir 28, 9303-9310.

Carn, F., Colin, A., Pitois, O., Vignes-Adler, M., Backov, R., 2009. Foam drainage in the presence of nanoparticle− surfactant mixtures. Langmuir 25, 7847-7856.

Chang, Y.-B., Lim, M., Pope, G., Sepehrnoori, K., 1994. CO2 flow patterns under multiphase flow: heterogeneous field-scale conditions. SPE Reservoir Engineering 9, 208-216.

Chen, S., Hou, Q., Zhu, Y., Wang, D., Li, W., 2014. On the origin of foam stability: understanding from viscoelasticity of foaming solutions and liquid films. Journal of dispersion science and technology 35, 1214-1221.

Cox, S., Neethling, S., Rossen, W., Schleifenbaum, W., Schmidt-Wellenburg, P., Cilliers, J., 2004. A theory of the effective yield stress of foam in porous media: the motion of a soap film traversing a three-dimensional pore. Colloids and Surfaces A: Physicochemical and Engineering Aspects 245, 143-151.

Derjaguin, B., Landau, L., 1993. Theory of the stability of strongly charged lyophobic sols and of the adhesion of strongly charged particles in solutions of electrolytes. Progress in Surface Science 43, 30-59.

Desarnaud, J., Bonn, D., Shahidzadeh, N., 2016. The pressure induced by salt crystallization in confinement. Scientific reports 6, 1-8.

Espinoza, D.A., Caldelas, F.M., Johnston, K.P., Bryant, S.L., Huh, C., 2010. Nanoparticle-stabilized supercritical CO2 foams for potential mobility control applications, SPE Improved Oil Recovery Symposium. Society of Petroleum Engineers.

Exerowa, D., Kruglyakov, P.M., 1997. Foam and foam films: theory, experiment, application. Elsevier.

Feng, C., Kong, Y., Jiang, G., Yang, J., Pu, C., Zhang, Y., 2012. Wettability modification of rock cores by fluorinated copolymer emulsion for the enhancement of gas and oil recovery. Applied Surface Science 258, 7075-7081.

Furuta, Y., Oikawa, N., Kurita, R., 2016. Close relationship between a dry-wet transition and a bubble rearrangement in two-dimensional foam. Scientific reports 6, 1-8.

Garcia, J.E., Pruess, K., 2003. Flow instabilities during injection of CO2 into salineaquifers. Ernest Orlando Lawrence Berkeley NationalLaboratory, Berkeley, CA (US).

Hirasaki, G., Miller, C., Szafranski, R., Lawson, J., Akiya, N., 1997a. Surfactant/foam process for aquifer remediation, International symposium on oilfield chemistry. Society of Petroleum Engineers.
Hirasaki, G., Miller, C., Szafranski, R., Tanzil, D., Lawson, J., Meinardus, H., Jin, M., Londergan, J., Jackson, R., Pope, G., 1997b. Field demonstration of the surfactant/foam process for aquifer remediation, SPE Annual Technical Conference and Exhibition. Society of Petroleum Engineers.
Hirasaki, G.J., Lawson, J., 1985. Mechanisms of foam flow in porous media: apparent viscosity in smooth capillaries. Society of Petroleum Engineers Journal 25, 176-190.
Horozov, T.S., 2008. Foams and foam films stabilised by solid particles. Current Opinion in Colloid & Interface Science 13, 134-140.
Jia, H., Huang, W., Han, Y., Wang, Q., Wang, S., Dai, J., Tian, Z., Wang, D., Yan, H., Lv, K., 2020. Systematic investigation on the interaction between SiO2 nanoparticles with different surface affinity and various surfactants. Journal of Molecular Liquids, 112777.
Jones, S., Van Der Bent, V., Farajzadeh, R., Rossen, W., Vincent-Bonnieu, S., 2016. Surfactant screening for foam EOR: Correlation between bulk and core-flood experiments. Colloids and Surfaces A: Physicochemical and Engineering Aspects 500, 166-176.
Kam, S., Rossen, W., 2003. A model for foam generation in homogeneous media. Spe Journal 8, 417-425.
Kantzas, A., Chatzis, I., Dullien, F., 1988. Enhanced oil recovery by inert gas injection, SPE enhanced oil recovery symposium. Society of Petroleum Engineers.
Karakashev, S.I., Ozdemir, O., Hampton, M.A., Nguyen, A.V., 2011. Formation and stability of foams stabilized by fine particles with similar size, contact angle and different shapes. Colloids and Surfaces A: Physicochemical and Engineering Aspects 382, 132-138.
Koczo, K., Lobo, L., Wasan, D., 1992. Effect of oil on foam stability: aqueous foams stabilized by emulsions. Journal of colloid and interface science 150, 492-506.
Kumar, S., Mandal, A., 2017. Investigation on stabilization of CO2 foam by ionic and nonionic surfactants in presence of different additives for application in enhanced oil recovery. Applied Surface Science 420, 9-20.
Lemlich, R., 1978. Prediction of changes in bubble size distribution due to interbubble gas diffusion in foam. Industrial & Engineering Chemistry Fundamentals 17, 89-93.
Lin, C.E., Wang, T.Z., Chiu, T.C., Hsueh, C.C., 1999. Determination of the critical micelle concentration of cationic surfactants by capillary electrophoresis. Journal of High Resolution Chromatography 22, 265-270.
Lobo, L., Nikolov, A., Wasan, D., 1989. Foam stability in the presence of oil: on the importance of the second virial coefficient. JOURNAL OF DISPERSION SCIENCE ANDTECHNOLOGY 10, 143-161.
Ma, K., Liontas, R., Conn, C.A., Hirasaki, G.J., Biswal, S.L., 2012. Visualization of improved sweep with foam in heterogeneous porous media using microfluidics. Soft Matter 8, 10669-10675.
Maestro, A., Rio, E., Drenckhan, W., Langevin, D., Salonen, A., 2014. Foams stabilised by mixtures of nanoparticles and oppositely charged surfactants: relationship between bubble shrinkage and foam coarsening. Soft Matter 10, 6975-6983.
Martinez, A.C., Rio, E., Delon, G., Saint-Jalmes, A., Langevin, D., Binks, B.P., 2008. On the origin of the remarkable stability of aqueous foams stabilised by nanoparticles: link with microscopic surface properties. Soft Matter 4, 1531-1535.

Nasr, N.H., Mahmood, S.M., Hematpur, H., 2019. A rigorous approach to analyze bulk and coreflood foam screening tests. Journal of Petroleum Exploration and Production Technology 9, 809-822.
Nikolov, A., Wasan, D., Huang, D., Edwards, D., 1986. The effect of oil on foam stability: mechanisms and implications for oil displacement by foam in porous media, SPE annual technical conference and exhibition. Society of Petroleum Engineers.
Osei-Bonsu, K., Grassia, P., Shokri, N., 2018. Effects of pore geometry on flowing foam dynamics in 3D-printed porous media. Transport in Porous Media 124, 903-917.
Osei-Bonsu, K., Shokri, N., Grassia, P., 2015. Foam stability in the presence and absence of hydrocarbons: From bubble-to bulk-scale. Colloids and Surfaces A: Physicochemical and Engineering Aspects 481, 514-526.
Osei-Bonsu, K., Shokri, N., Grassia, P., 2016. Fundamental investigation of foam flow in a liquid-filled Hele-Shaw cell. Journal of colloid and interface science 462, 288-296.
Panthi, K., Singh, R., Mohanty, K.K., 2017. Microencapsulation and stimuli-responsive controlled release of particles using water-in-air powders. Langmuir 33, 3998-4010.
Rossen, W.R., 1990. Theory of mobilization pressure gradient of flowing foams in porous media: I. Incompressible foam. Journal of colloid and interface science 136, 1-16.
Rossen, W.R., 1996. Foams in enhanced oil recovery. Foams: theory, measurements and applications 57, 413-464.
Saint-Jalmes, A., 2006. Physical chemistry in foam drainage and coarsening. Soft Matter 2, 836-849.
Shojaei, M.J., de Castro, A.R., Méheust, Y., Shokri, N., 2019. Dynamics of foam flow in a rock fracture: Effects of aperture variation on apparent shear viscosity and bubble morphology. Journal of colloid and interface science 552, 464-475.
Shojaei, M.J., Osei-Bonsu, K., Grassia, P., Shokri, N., 2018a. Foam flow investigation in 3D-printed porous media: fingering and gravitational effects. Industrial & Engineering Chemistry Research 57, 7275-7281.
Shojaei, M.J., Osei-Bonsu, K., Richman, S., Grassia, P., Shokri, N., 2018b. Foam stability influenced by displaced fluids and by pore size of porous media. Industrial & Engineering Chemistry Research 58, 1068-1074.
Singh, R., Mohanty, K.K., 2015. Synergy between nanoparticles and surfactants in stabilizing foams for oil recovery. Energy & Fuels 29, 467-479.
Singh, R., Mohanty, K.K., 2017. Nanoparticle-stabilized foams for high-temperature, high-salinity oil reservoirs, SPE Annual Technical Conference and Exhibition. Society of Petroleum Engineers.
Talebian, S.H., Masoudi, R., Tan, I.M., Zitha, P.L., 2013. Foam assisted CO2-EOR; concepts, challenges and applications, SPE Enhanced Oil Recovery Conference. Society of Petroleum Engineers.
Vatanparast, H., Shahabi, F., Bahramian, A., Javadi, A., Miller, R., 2018. The role of electrostatic repulsion on increasing surface activity of anionic surfactants in the presence of hydrophilic silica nanoparticles. Scientific reports 8, 1-11.
Verwey, E.J.W., Overbeek, J.T.G., 1955. Theory of the stability of lyophobic colloids. Journal of Colloid Science 10, 224-225.
Yekeen, N., Manan, M.A., Idris, A.K., Padmanabhan, E., Junin, R., Samin, A.M., Gbadamosi, A.O., Oguamah, I., 2018. A comprehensive review of experimental studies of nanoparticles-stabilized foam for enhanced oil recovery. Journal of Petroleum Science and Engineering 164, 43-74.
Yu, D., Huang, F., Xu, H., 2012a. Determination of critical concentrations by synchronous fluorescence spectrometry. Analytical Methods 4, 47-49.

Yu, J., An, C., Mo, D., Liu, N., Lee, R.L., 2012b. Foam mobility control for nanoparticle-stabilized supercritical CO2 foam, SPE improved oil recovery symposium. Society of Petroleum Engineers.
Yusuf, S., Manan, M., Zaidi Jaafar, M., 2013. Aqueous foams stabilized by hydrophilic silica nanoparticles via in-situ physisorption of nonionic TX100 Surfactant. Iranian Journal of Energy and Environment 4, 0-0.
Zhang, T., Roberts, M., Bryant, S.L., Huh, C., 2009. Foams and emulsions stabilized with nanoparticles for potential conformance control applications, SPE international symposium on oilfield chemistry. Society of Petroleum Engineers.